CORROSION SCIENCE AND TECHNOLOGY, Vol.21, No.1(2022), pp.53~61
[Research Paper]
pISSN 1598-6462 / eISSN 2288-6524
DOI: https://doi.org/10.14773/cst.2022.21.1.53

Oxidation of Fe-(5.3-29.8)%Mn-(1.1-1.9)%Al-0.45%C Alloys at 550-650 °C

Soon Yong Park[1], Xiao Xiao[2], Min Ji Kim[3], Geun Taek Lee[1], Dae Ho Hwang[1], Young Ho Woo[1], and Dong Bok Lee[2,†]

[1]*R&D Center, PIM KOREA, Daegu, 42921, Korea*
[2]*School of Advanced Materials Science and Engineering, Sungkyunkwan University, Suwon, 16419, Korea*
[3]*School of Advanced Materials Application, Korea Polytechnics, Incheon, 21417, Korea*
(Received October 06, 2021; Revised October 21, 2021; Accepted January 06, 2022)

Alloys of Fe-(5.3-29.8)%Mn-(1.1-1.9)%Al-(0.4-0.5)%C were oxidized at 550 °C to 650 °C for 20 h to understand effects of alloying elements on oxidation. Their oxidation resistance increased with increasing Mn level to a small extent. Their oxidation kinetics changed from parabolic to linear when Mn content was decreased and temperature was increasing. Oxide scales primarily consisted of Fe_2O_3, Mn_2O_3, and $MnFe_2O_4$ without any protective Al-bearing oxides. During oxidation, Fe, Mn, and a lesser amount of Al diffused outward, while oxygen diffused inward to form internal oxides. Both oxide scales and internal oxides consisted of Fe, Mn, and a small amount of Al. The oxidation of Mn and carbon transformed γ-matrix to α-matrix in the subscale. The oxidation led to the formation of relatively thick oxide scales due to inherently inferior oxidation resistance of alloys and the formation of voids and cracks due to evaporation of manganese, decarburization, and outward diffusion of cations across oxides.

Keywords: *High-Mn steel, Oxidation, Oxide scale, Iron, Manganese*

1. Introduction

Fe-Mn-Al-C alloys have attracted much interest in the last decades as potential candidates to replace the costly Fe-Ni-Cr stainless steels because of their cost effectiveness, high strength, good formability, tensile strength, low density, and low-temperature properties [1,2]. Their microstructures and mechanical properties have been actively studied for applications in automobiles and oil and gas exploration [3-5]. Previously, oxidation studies were performed in the composition range of Fe-(1-32)Mn-(1.5-16)Al-(0-1)C in a temperature range of 600-1250 °C in air or oxygen [6-11]. All chemistry values are in weight percent unless otherwise specified. The oxidation of Fe-(7.5-30.1)Mn-(5-16)Al-(0, 0.77)C at 600-1000 °C led to the formation of an alumina layer interrupted by nodules that consisted mostly of manganese oxide [6,7], and needle-like AlN precipitated beneath these nodules [7]. The oxidation of Fe-31Mn-9Al-0.87C at 800 - 1100 °C resulted in formation of the outer $(Mn,Fe)_2O_3$-rich and inner $(Mn,Fe)_3O_4$-rich layer [8,9], whereas that of Fe-32Mn-7.5Al-0.6C at 1000 °C led to the formation of a discontinuous alumina layer interspersed with a less protective $MnAl_2O_4$ spinel [10]. Fe-30Mn-5Al-0.5C formed the oxide scale consisting of a thin surface Mn_2O_3 film, a thick $MnFe_2O_4$ layer, and an internal oxidation zone at 600 - 900 °C [11]. As was stated above, diverse kinds of oxides, scale morphologies, and dominant oxidation processes were reported depending on the alloy composition and oxidation conditions.

This study aims at characterizing the oxidation behavior of a new kind of lightweight Fe-Mn-Al-C alloys and comparing the results with the results obtained from oxidation of iron and manganese. It is noted that oxidation studies on manganese are scarce because manganese is usually used as an alloying element [12-14]. In the present work, Fe-(5.29-29.8)Mn-(1.09-1.89)Al-(0.44, 0.45)C alloys were manufactured and oxidized at 550 - 650 °C for 20 h. Such an oxidation condition was selected because stress-relieving temperature of Fe-Mn-Al-C alloys, which were welded with other low alloy steels in automobile applications, lies in the range of 500 - 700 °C for 10-40 h

†Corresponding author: dlee@skku.ac.kr
Soon Yong Park: Researcher, Xiao Xiao: Master, Min Ji Kim: Professor, Geun Taek Lee: Researcher, Dae Ho Hwang: Researcher, Young Ho Woo: Researcher, Dong Bok Lee: Professor

Table 1. Chemical composition of Fe-Mn-Al-C alloys

Designation	Composition (wt%)
5.3Mn	Fe-5.29Mn-1.89Al-0.45C
10.2Mn	Fe-10.20Mn-1.85Al-0.45C
15.1Mn	Fe-15.06Mn-1.60Al-0.44C
20.4Mn	Fe-20.38Mn-1.49Al-0.45C
25.9Mn	Fe-25.91Mn-1.27Al-0.45C
29.8Mn	Fe-29.80Mn-1.09Al-0.44C

[5,6]. The effect of chemical compositions of Fe-Mn-Al-C alloys on oxidation was discussed in this study.

2. Experimental Methods

Table 1 lists the chemical composition of six different Fe-Mn-Al-C alloys. The alloy compositions were designed to achieve high strength and good formability with high elongation for automotive applications. The alloys were induction-melted under vacuum, cast into slabs with a 6 cm thickness, reheated at 1200 ºC for 1 h, hot rolled to a 3 mm thickness, water quenched to 650 ºC, homogenized at 650 ºC for 1 h, and then cooled to room temperature. They were cut into 10 mm × 10 mm × 3 mm coupons, ground to 1000-grit with abrasive paper to remove surface scales, ultrasonically cleaned in acetone and alcohol, and oxidized at 550, 600, and 650 ºC for 20 h in atmospheric air using a thermogravimetric analyzer. For comparison purposes, 99.9% pure Fe and Mn sheets were also oxidized. The oxidized specimens were inspected using a scanning electron microscope (SEM) equipped with an energy-dispersive spectrometer (EDS), an electron probe microanalyzer (EPMA), and an X-ray diffractometer (XRD) with Cu-Kα radiation at 40 kV and 150 mA.

3. Results and Discussion

Fig. 1 shows XRD patterns of Fe-Mn-Al-C alloys. Here, 5.3%Mn was ferritic, and 10.2%Mn was mixed with ferrite and austenite. As the Mn level increased from 10.2% to 15.1%, the diffraction intensity of ferrite decreased, while that of austenite increased. Only austenite was detected for (20.4, 25.9, 29.8)% Mn, because the concentration of austenite-stabilizing manganese increased, whereas that of ferrite-stabilizing

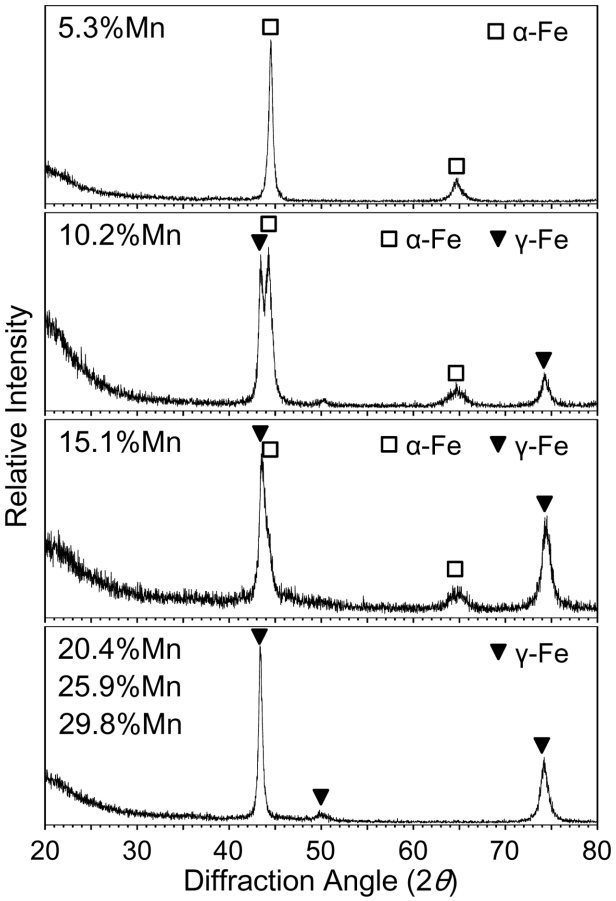

Fig. 1. XRD patterns of Fe-Mn-Al-C alloys

aluminum decreased.

Fig. 2 shows oxidation curves of Fe, Mn, and Fe-Mn-Al-C alloys at 550 - 650 ºC. Generally, weight gain increased with increasing oxidation time and temperature due to the enhanced reaction and diffusion rate. At 550 ºC, iron oxidized parabolically, whereas manganese suffered accelerated oxidation at 13.8 h owing to breakage of its oxide scale. At 550 ºC, 5.3Mn oxidized linearly, (10.2, 15.1, 20.4)Mn oxidized almost parabolically after initial transient period of 2.5 h, and (25.9, 29.8)Mn suffered partial scale spallation at (17.3, 14) h, respectively, owing to insufficient oxide plasticity. At 600 and 650 ºC, oxidation curves were smooth, mainly because the plasticity of oxide scales increased at higher temperatures. Additional minor reason was the eclipse of small weight fluctuations due to local scale breakage/spallation by large weight gains. At 550 - 650 ºC, iron and manganese gained more weights than Fe-Mn-Al-C alloys. Completely different oxide scales formed on iron, manganese, and Fe-Mn-Al-

C alloys, as will be shown later. Generally, high-Mn alloys gained less weights than low-Mn alloys, although the former had lower amounts of aluminum than the latter. At each oxidation temperature, high-Mn and low-Mn alloys tended to follow parabolic and linear oxidation kinetics, respectively. Hence, it is seen that Mn beneficially increased the isothermal oxidation resistance of current alloys. However, some authors have suggested that manganese and carbon decreased the oxidation resistance of Fe-Mn(-Al-C(-Cr)) alloys due to decarburization and the selective oxidation of manganese [6,8,15,16]. Such apparent discrepancy between this paper and previous studies is mainly due to the different levels of the alloying elements, which generated dissimilar scale microstructures consisting of diverse oxides, depending on the alloy composition. For example, ours had (1.1-1.9)Al, while others had (5-16)Al. Resultantly, ours did not form any Al-bearing oxides according to the XRD analysis, while others reported the formation of Al_2O_3, (Fe, Mn)Al_2O_4, and/or $MnAl_2O_4$ [6,8,15,16]. Previously, manganese was explained to be more oxidation resistant than iron [6]. However, this study indicated that the oxidation resistances of both manganese and iron was poor, and the difference between them was considered to be marginal.

Assuming that the parabolic oxidation law is obeyed for the sake of simplicity, the oxidation curves shown in Fig. 2 were fitted to the equation $\Delta W^2 = k_p t$, where ΔW is the weight gain per unit area, t is the oxidation time, and k_p is the parabolic rate constant. The deviation of Fig. 2 from the parabolic oxidation law resulted from experimental scattering, partial scale detachment/spallation, and gradual transition from parabolic to linear oxidation with increasing the temperature and decreasing Mn level in Fe-Mn-Al-C alloys. Values of k_p of Fe-Mn-Al-C alloys were measured for the oxidation period of 2.5-20 h, excluding the initial transient period. Also, the oxidation data of (Mn after 13.8 h), (25.9Mn after 17.3 h), and (29.8Mn after 14 h) at 550 °C were disregarded due to accelerated oxidation, or partial spallation of oxide scales. Fig. 3 indicate that manganese oxidized slightly more slowly than iron. The oxidation resistance of Fe-Mn-Al-C alloys increased with increasing Mn level to a small extent. Our k_p values of iron and manganese were reasonably located around those of iron and manganese

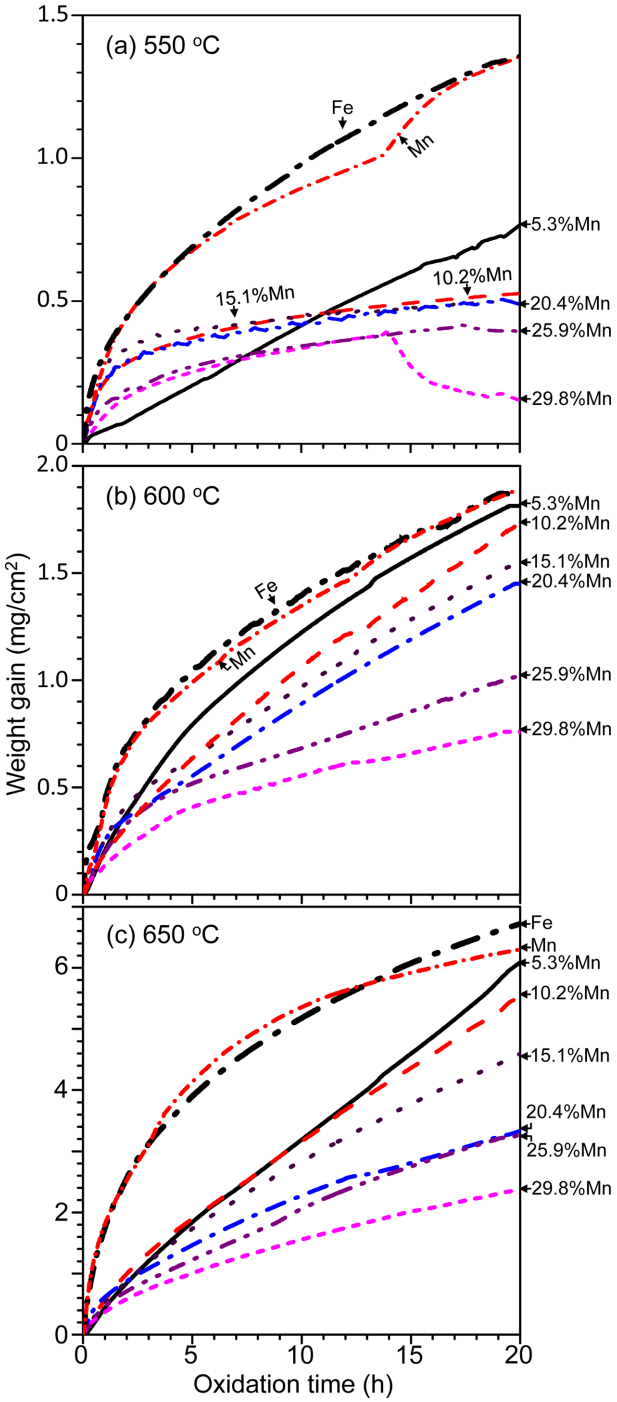

Fig. 2. Oxidation curves of Fe, Mn, and Fe-Mn-Al-C alloys at (a) 550 °C, (b) 600 °C, (c) 650 °C

reported previously [13,14,17,18]. Values of k_p of manganese in air reported by Buscail and Larpin were too low [12]. Those of iron in 1 atm of oxygen or air, which were compiled by Bertrand et. al. [18] indicated that they were broadly independent of oxygen pressure.

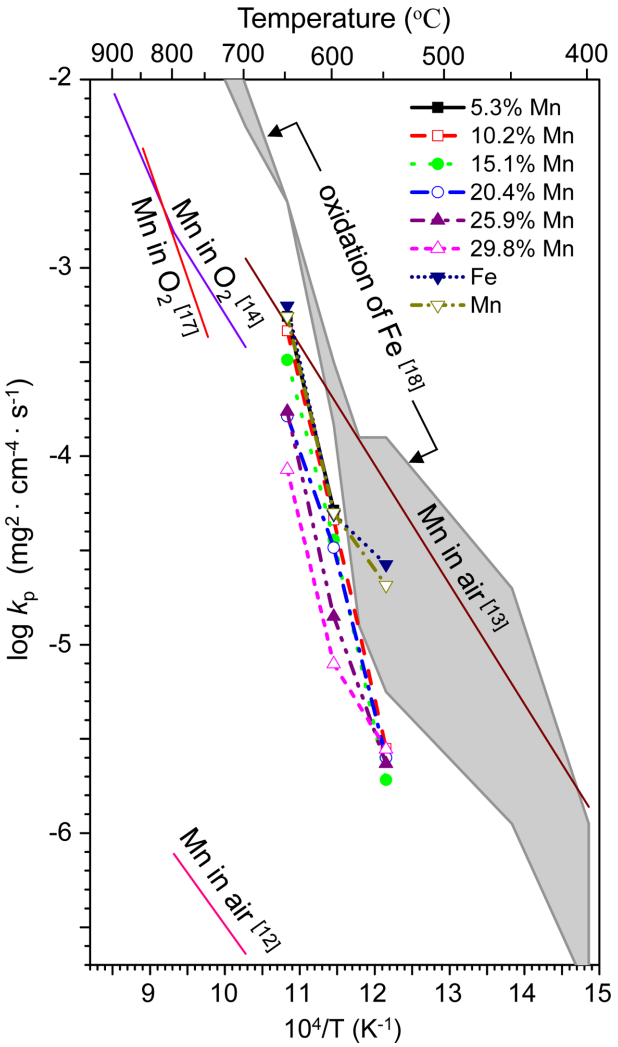

Fig. 3. Arrhenius plot of parabolic rate constants for the oxidation of Fe, Mn, and Fe-Mn-Al-C alloys. The k_p values for the oxidation of manganese in 1 atm of air [12,13] and oxygen [14,17] as well as iron in 1 atm of air and oxygen [18] are superimposed

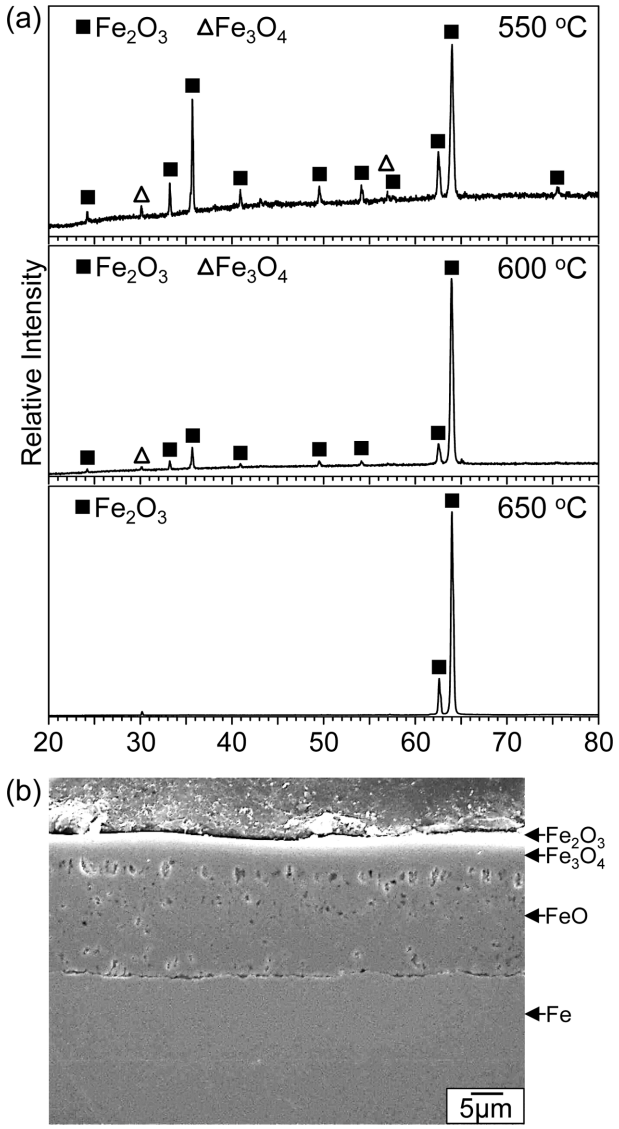

Fig. 4. Iron oxidized for 20 h. (a) XRD patterns at 550, 600, and 650 °C, (b) cross-sectional SEM image at 600 °C

When iron is exposed to air above 570 °C, it grows a scale consisting of an inner, thick FeO layer, an intermediate, thin Fe_3O_4 layer, and an outer, extremely thin Fe_2O_3 layer, because nonstoichiometric $Fe_{1-x}O$ grows much faster than stoichiometric Fe_3O_4 and Fe_2O_3 [18,19]. Below 570 °C, FeO is unstable so that an inner, thin Fe_3O_4 layer, and an outer, thinner Fe_2O_3 layer form. The growth of FeO, Fe_3O_4 and Fe_2O_3 is primarily governed by the diffusion of Fe^{2+}, (Fe^{2+}, Fe^{3+}), and (Fe^{3+}, O^{2-}) ions, respectively [18,19]. At 550 - 650 °C, the intensity of the XRD pattern of the outer Fe_2O_3 layer was stronger than that of the underlying Fe_3O_4 layer (Fig. 4a). FeO was not detected in this figure because of its instability at 550 °C, and the presence of overlaying Fe_3O_4/Fe_2O_3 layer at 600 - 650 °C. The outward diffusion of Fe^{2+} ions from the FeO/Fe interface toward the FeO/Fe_3O_4 interface accompanies the counter-diffusion of cation vacancies toward the FeO/Fe interface [19]. Hence, the fast growing FeO layer had numerous voids, reflecting a high cation-vacancy concentration (Fig. 4b).

Manganese oxidizes in a manner similar to iron, forming multi-layer scales. It forms an inner, thick MnO layer, an intermediate, a less thick Mn_3O_4 layer, and an outer, thin Mn_2O_3 layer [12]. Mn_2O_3 becomes unstable above 880 °C. Like FeO, MnO exhibits a relatively large deviation from stoichiometry. $Mn_{1-x}O$ grows faster than

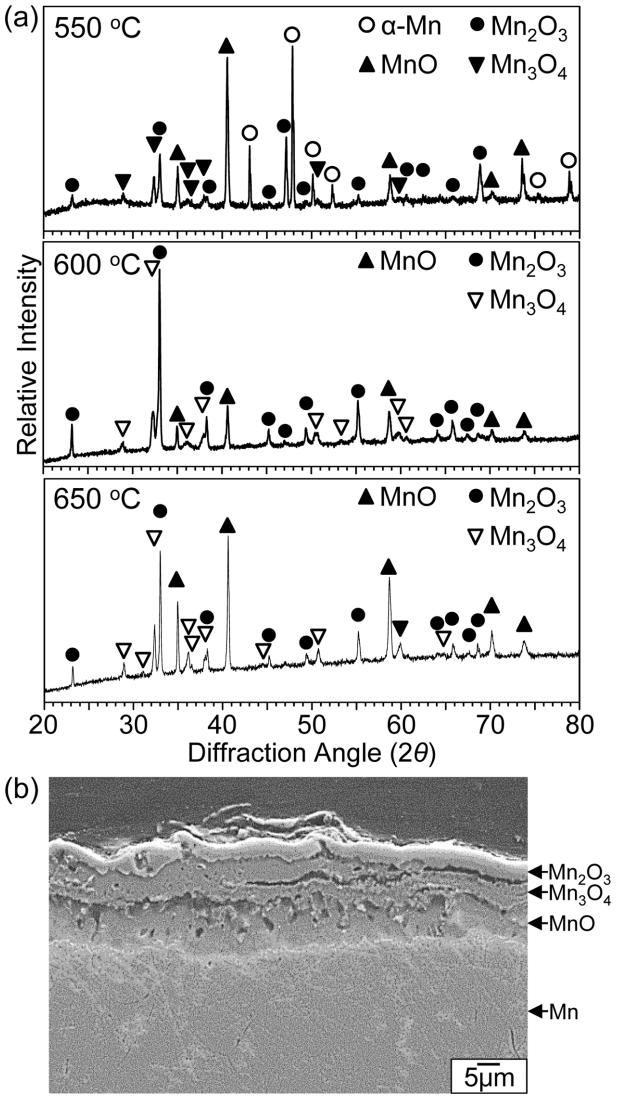

Fig. 5. Manganese oxidized for 20 h. (a) XRD patterns at 550, 600, and 650 °C, (b) cross-sectional SEM image at 600 °C

$Mn_{3-y}O_4$ or Mn_2O_{3-z} [20]. Fig. 5a indicates the formation of MnO, Mn_3O_4, and Mn_2O_3 at 550 - 650 °C. At 550 °C, strong α-Mn peaks were additionally detected due to partial spallation of the oxide scale during the scaling and subsequent cooling stage. A non-uniform, and loosely adherent oxide scale was shown in Fig. 5b. The outer Mn_2O_3 layer convoluted and partially detached due to the developed growth and thermal stress. When manganese is oxidized primarily by the outward diffusion of cations, cation vacancies form to generate voids, especially in the MnO layer [21]. Manganese, whose vapor pressure is much higher than that of iron or aluminum, also diffuses outward through voids. For example, the equilibrium vapor pressures of Mn, Fe, and Al are calculated as 1.86×10^{-10}, 1.16×10^{-17}, and 1.88×10^{-13} (atm) at 600 °C, respectively, from the thermodynamic data [22]. Fast oxidation, void formation, local cracking, and spallation of the oxide scales were the characteristics of Mn oxidation (Fig. 5b).

Fig. 6 shows the XRD/SEM/EPMA results of 10.2 Mn after oxidation at 650 °C for 20 h. The intensity of the XRD pattern shown in Fig. 6a decreased in the order of Fe_2O_3, Mn_2O_3, and $MnFe_2O_4$. Hematite reacted partially with MnO to yield the $MnFe_2O_4$ spinel. Higher manganese levels formed more manganese oxides and $MnFe_2O_4$. The $MnFe_2O_4$ spinel might grow more slowly than manganese- or iron-oxides. It might play a major role in improving the oxidation resistance of Fe-Mn-Al-C alloys (Fig. 2). Nonetheless, oxidation resistance of Fe-Mn-Al-C alloys was inferior, because the oxide scales were mixed with Fe_2O_3, Mn_2O_3, and $MnFe_2O_4$. The platinum wire, both end of which was spot welded on the alloy surface prior to oxidation for good contact, was found above the inner oxide scale (Fig. 6b). This marker test indicates that the outer and inner oxide scale were formed by the outward diffusion of cations and oxygen ions, respectively. The 40 μm-thick outer scale was detached from the 30 μm-thick inner scale to relieve thermal and growth stresses generated during oxidation and subsequent cooling. The enlarged cross-sectional EPMA image and corresponding elemental maps of the oxide scale are shown in Fig. 6c and d, respectively. Detachment of the outer scale from the inner scale was accompanied by the cracking at the bottom of the outer oxide scale (Fig. 6c). The outer scale was enriched with Fe, Mn, and Al (Fig. 6d). Manganese diffused outward strongly into the outer scale, which was assisted by its evaporation and relatively rapid rate of diffusion across the scale. Strong outward diffusion of manganese was similarly reported from the high-temperature oxidation of Fe-30.1Mn-9.7Al-0.77C alloy [7], Fe-30Mn-5Al-0.5C alloy [11], and Fe-28Cr-1Mn alloy [23]. Aluminum diffused outward weakly due to its low concentration in the alloy, and low diffusivity in oxides resulting from its high oxygen affinity. On the other hand, the absence of any Al-bearing oxides in Fig. 6a was attributed to their small amount, or dissolution in other oxides. For example, Al_2O_3 can dissolve in Fe_2O_3 and Mn_2O_3 up to ~ 5 and 10%, respectively. Inwardly diffusing

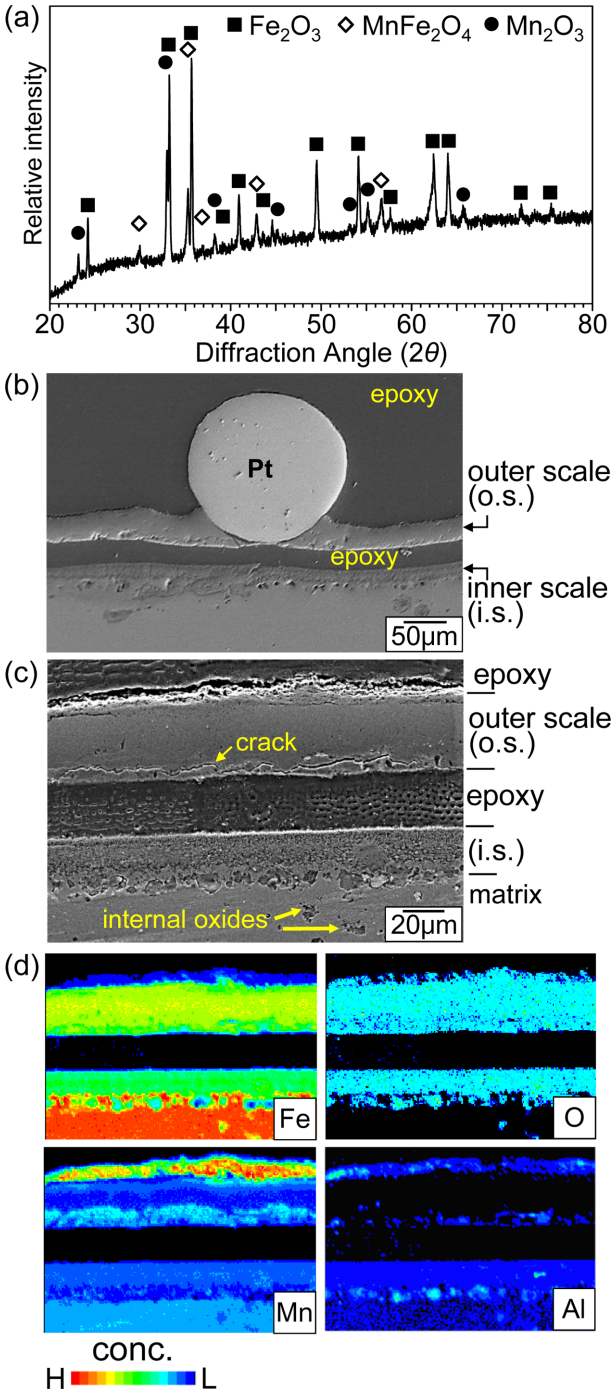

Fig. 6. Fe-10.2Mn-1.9Al-0.5C alloy after oxidation at 650 °C for 20 h. (a) XRD pattern, (b) SEM cross-sectional image, (c) EPMA cross-sectional image, (d) EPMA maps of (c)

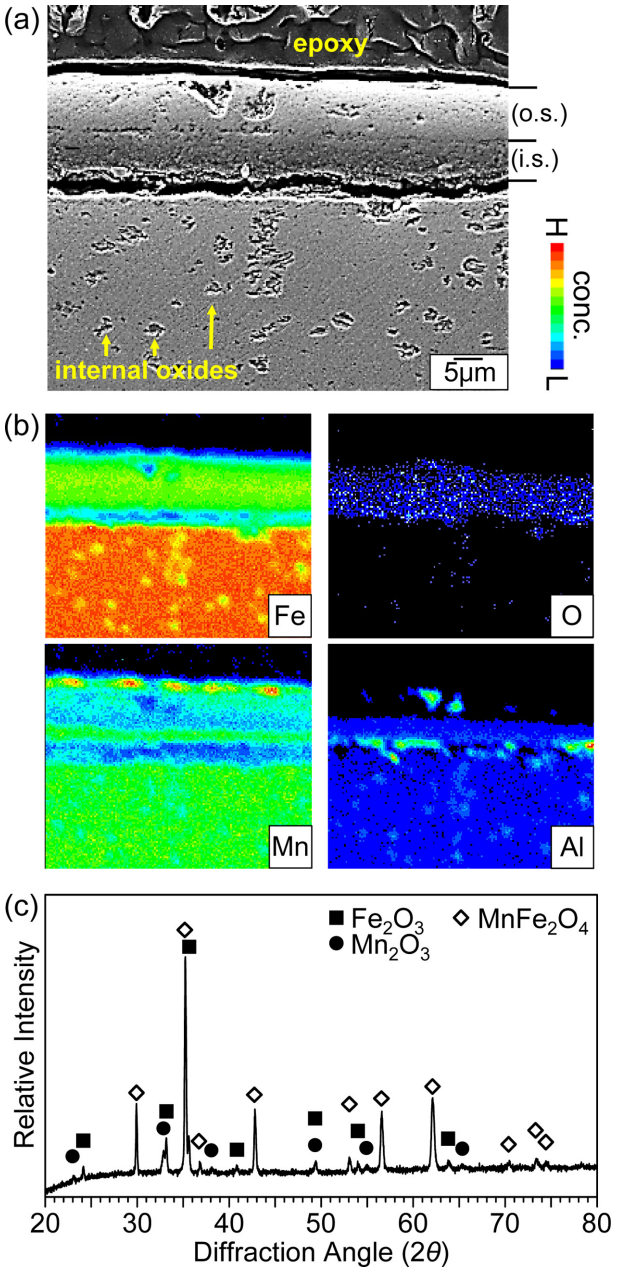

Fig. 7. Fe-10.2Mn-1.9Al-0.5C alloy after oxidation at 600 °C for 20 h. (a) EPMA cross-sectional image, (b) EPMA maps of (a), (c) XRD pattern of the oxide scale

oxygen ions formed the (Fe, Mn, Al)-mixed inner oxide scale and internal oxides. Internal oxidation of aluminum hindered the outward diffusion of aluminum and the buildup of the Al-bearing protective oxide layer. Spallation and delamination of the oxide scale facilitated internal oxidation.

Fig. 7 shows the EPMA/XRD results of 10.2Mn after oxidation at 600 °C for 20 h. The thickness of the oxide scale decreased to 17 μm (Fig. 7a). The oxide scale consisted of Fe, Mn, and a lower amount of Al (Fig. 7b). This figure indicates that more Mn diffused outward to the top surface than Al, making the figure analogous to Fig. 6d. Again, the outward diffusion of Al was limited due to the low Al levels in the alloy and the strong oxygen

affinity of Al. Manganese was unevenly distributed in the scale, and it was depleted in the subscale because of its strong tendency to diffuse outward. Both the oxide scale and internal oxides consisted of Fe, Mn, and Al. Unlike Fig. 6b, Fig. 7a shows that the bi-layered oxide scale was not yet split into two, because a thinner oxide scale formed. The oxide scale was loosely adherent, due to accumulated growth and thermal stress, voids that formed by the outward diffusion of cations, evaporation of Mn, and decarburization of the alloy [9]. The XRD pattern shown in Fig. 7c indicates that the intensity decreased in the order of $MnFe_2O_4$, Fe_2O_3, and Mn_2O_3. Again, Al-bearing oxides such as Al_2O_3, $FeAl_2O_4$, and $MnAl_2O_4$, which were found in Fe-31Mn-9Al-0.87C alloys after oxidation at 800 - 1100 °C [13] were absent due to their small amount, and/or the dissolution of Al_2O_3 in isostructural Fe_2O_3.

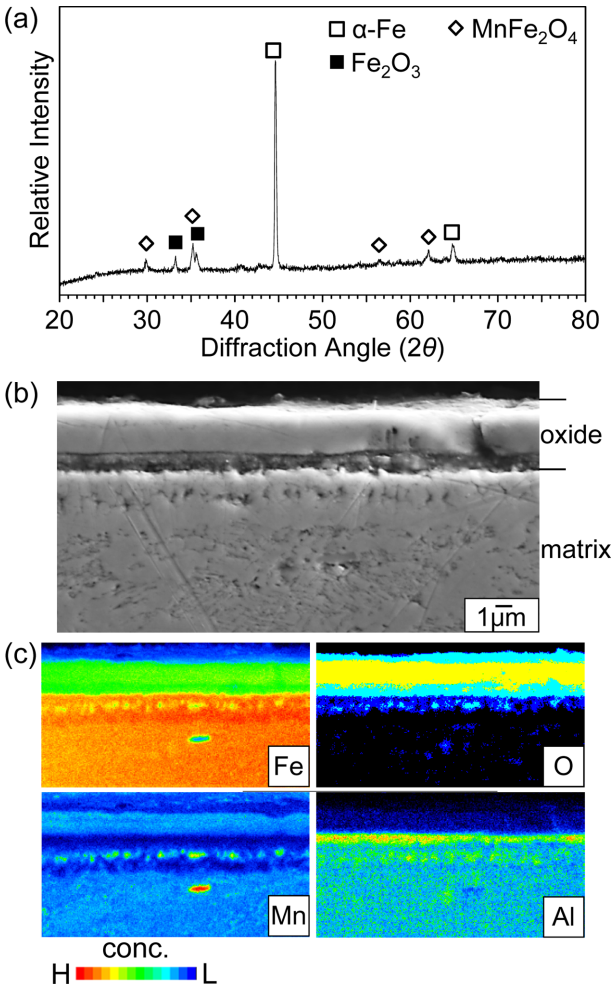

Fig. 8. Fe-10.2Mn-1.9Al-0.5C alloy after oxidation at 550 °C for 20 h. (a) XRD pattern, (b) EPMA cross-sectional image, (c) EPMA maps of (b)

The alloy outlined in Figs. 6 and 7 was oxidized at 550 °C and analyzed using XRD/EPMA. The results are shown in Fig. 8. The α-Fe matrix was strongly detected since the oxide scale consisting of Fe_2O_3 and $MnFe_2O_4$ was thin (Fig. 8a). Mn_2O_3 was no longer detected, due to its small amount or dissolution in Fe_2O_3, which can dissolve up to 5% Mn_2O_3 [24]. No Al-bearing oxides were detected. The oxide scale was 4 μm-thick and did not yet develop into bi-layered oxide scale (Fig. 8b). It consisted of Fe, Mn, and a lower amount of Al (Fig. 8c). Again, manganese diffused outward into the oxide scale more strongly than aluminum, reflecting its high diffusivity in the oxide scale. This resulted in the enrichment of aluminum and the depletion of manganese around the scale/matrix interface, below which oxygen dissolved to a certain extent. In this study, competitive oxidation of Fe, Mn, Al, and possibly carbon was unavoidable due mainly to absence of a protective barrier oxide layer.

4. Conclusions

The Fe-5.3Mn-1.9Al-0.5C alloy was ferritic, Fe-(10.2-15.1)Mn-(1.6-1.9)Al-(0.4-0.5)C alloys consisted primarily of ferrite and austenite, while Fe-(20.4-29.8)Mn-(1.1-1.5)Al-(0.4-0.5)C alloys were austenitic. All these alloys oxidized relatively fast to Fe_2O_3, Mn_2O_3, and $MnFe_2O_4$ at 550 - 650 °C. They oxidized more slowly than iron and manganese. Manganese that formed MnO, Mn_3O_4, and Mn_2O_3 oxidized slightly more slowly than iron that formed FeO, Fe_3O_4, and Fe_2O_3. High-Mn alloys displayed better oxidation resistance than low-Mn alloys, indicating that manganese was beneficial due to the formation of an increased amount of $MnFe_2O_4$ spinel. The growth of outer and inner oxide scales was governed by the outward diffusion of (Fe^{2+}, Fe^{3+}, Mn^{2+}, Mn^{3+}, Al^{3+})-ions and inward diffusion of O^{2-} ions, respectively. The outward diffusion of cations, volume expansion caused by the formation of oxides, vaporization of manganese, and decarburization generated pores and cracks in scales. Inward diffusion of anions resulted in the formation of the inner oxide layer and internal oxides consisting of Fe, Mn, and Al. These elements also made up the outer oxide layer.

Acknowledgements

This work was supported by 2021 Chasedae Sundo Kisul Gaebal Saup supported by Daegu Technopark.

References

1. S. O. Kim, J. K. Hwang, and S. J. Kim, Effect of Alloying Elements (Cu, Al, Si) on the Electrochemical Corrosion Behaviors of TWIP Steel in a 3.5 % NaCl Solution, *Corrosion Science and Technology,* **18**, 300 (2019). Doi: https://doi.org/10.14773/cst.2019.18.6.300
2. S. H. Kim, J. Y. Huh, M. S. Kim, and J. S. Kim, Effects of Oxygen Partial Pressure on Oxidation Behavior of CMnSi TRIP Steel in an Oxidation-Reduction Scheme, *Corrosion Science and Technology,* **16**, 15 (2017). Doi: https://doi.org/10.14773/cst.2017.16.1.15
3. O. Bouaziz, S. Allain, C. Scott, P. Cugy, and D. Barbier, High Manganese Austenitic Twinning Induced Plasticity Steels: A Review of the Microstructure Properties Relationships, *Current Opinion in Solid State and Materials Science*, **15**, 141 (2011). Doi: https://doi.org/10.1016/j.cossms.2011.04.002
4. S. W. Park, J. Y. Park, K. M. Cho, J. H. Jang, S. J. Park, J. Moon, T. H. Lee, and J. H. Shin, Effect of Mn and C on Age Hardening of Fe–Mn–Al–C Lightweight Steels, *Metals and Materials International*, **25**, 683 (2019). Doi: https://doi.org/10.1007/s12540-018-00230-x
5. J. Moon, S. J. Park, and C. H. Lee, Current Status on Development of Lightweight Steels and Welding Characteristics, *Journal of Welding and Joining*, **38**, 333 (2020). Doi: https://doi.org/10.5781/JWJ.2020.38.4.1
6. P. R. S. Jackson and G. R. Wallwork, High Temperature Oxidation of Iron-Manganese-Aluminum Based Alloys, *Oxidation of Metals*, **21**, 135 (1984). Doi: https://doi.org/10.1007/bf00741468
7. C. J. Wang and Y. C. Chang, Formation and Growth Morphology of Nodules in the High-Temperature Oxidation of Fe-Mn-Al-C Alloy, *Materials Chemistry and Physics*, **77**, 738 (2003). Doi: https://doi.org/10.1016/S0254-0584(02)00134-7
8. J. G. Duh and C. J. Wang, Formation and Growth Morphology of Oxidation-induced Ferrite Layer in Fe-Mn-Al-Cr-C Alloys, *Journal of Materials Science*, **25**, 2063 (1990). Doi: https://doi.org/10.1007/BF01045765
9. J. G. Duh and C. J. Wang, High Temperature Oxidation of Fe-31 Mn-9Al-xCr-0.87C Alloys (x = 0, 3 and 6), *Journal of Materials Science*, **25**, 268 (1990). Doi: https://doi.org/10.1007/BF00544219
10. J. P. Sauer, R. A. Rapp, and J. P. Hirth, Oxidation of Iron-Manganese-Aluminum Alloys at 850 and 1000 °C, *Oxidation of Metals*, **18,** 285 (1982). Doi: https://doi.org/10.1007/BF00656572
11. P. Pérez, F. J. Pérez, C. Gómez, and P. Adevaa, Oxidation Behaviour of an Austenitic Fe–30Mn–5Al–0.5C Alloy, *Corrosion Science*, **44**, 113 (2002). Doi: https://doi.org/10.1016/S0010-938X(01)00043-9
12. H. Buscail and J. P. Larpin, The Influence of Ceria Surface Additions on Manganese Oxidation at High Temperatures, *Oxidation of Metals*, **43**, 237 (1995). Doi: https://doi.org/10.1007/BF01047029
13. E. B. Evans, C. A. Phalnikar, and W. M. Baldwin, High Temperature Scaling of Nickel-Manganese Alloys, *Journal of the Electrochemical Society*, **103**, 367 (1956). Doi: https://doi.org/10.1149/1.2430358
14. F. Gesmundo, C. de Asmundis, and C. Bottino, High-Temperature Corrosion of Manganese in Pure SO_2, *Oxidation of Metals*, **14**, 15 (1980). Doi: https://doi.org/10.1007/BF00604101
15. V. D. F. C. Lins, M. A. Freitas, and E. M. D. P. e Silva, Oxidation Kinetics of an Fe-31.8Mn-6.09Al-1.60Si-0.40C Alloys at Temperature from 600 to 900 °C, *Corrosion Science*, **46**, 1895 (2004). Doi: http://doi.org/10.1016/j.corsci.2003.10.015
16. J. G. Duh, J. W. Lee, and C. J. Wang, Microstructural Development in the Oxidation-induced Phase Transformation of Fe-Al-Cr-Mn-C Alloys, *Journal of Materials Science*, **23**, 2649 (1988). Doi: https://doi.org/10.1007/BF01111928
17. F. Gesmundo, P. Nanni, and D. P. Whittle, High Temperature Oxidation of Co-Mn Alloys, *Corrosion Science*, **19**, 675 (1979). Doi: https://doi.org/10.1016/S0010-938X(79)80140-7
18. N. Bertrand, C. Desgranges, D. Poquillon, M. C. Lafont, and D. Monceau, Iron Oxidation at Low Temperature (260–500 °C) in Air and the Effect of Water Vapor, *Oxidation of Metals*, **73**, 139 (2010). Doi: https://doi.org/10.1007/s11085-009-9171-0
19. N. Birks and G. H. Meier, Introduction to High Temperature Oxidation of Metals, p.72, Edward Arnold, London (1983). Doi: https://doi.org/10.1017/CBO9781139163903
20. L. Kjellqvist and M. Selleby, Thermodynamic Assessment of the Fe-Mn-O System, *Journal of Phase Equilibria and Diffusion*, **31**, 113 (2010). Doi: https://doi.org/

10.1007/s11669-009-9643-6

21. K. Fueki and J. B. Wagner, Oxidation of Manganese in CO_2-CO Mixtures, *Journal of The Electrochemical Society*, **112**, 970 (1965). Doi: https://doi.org/10.1149/1.2423353
22. I. Barin, *Thermochemical Data of Pure Substances, 3rd ed.*, VCH, Germany (1989). Doi: https://doi.org/10.1002/9783527619825
23. F. H. Stott, F. I. Wei, and C. A. Enahoro, The Influence of Manganese on the High-Temperature Oxidation of Iron-chromium Alloys, *Materials and Corrosion*, **40**, 198 (1989). Doi: https://doi.org/10.1002/maco.19890400403
24. A. Muan and S. Somiya, The System Iron Oxide-Manganese Oxide in Air, *American Journal of Science*, **260**, 230 (1962). Doi: https://doi.org/10.2475/ajs.260.3.230